THE ASTROPHYSICAL JOURNAL, 479:497–503, 1997 April 10

ELECTRON-ION RECOMBINATION OF NEUTRAL IRON

SULTANA N. NAHAR, MANUEL A. BAUTISTA, AND ANIL K. PRADHAN
Department of Astronomy, The Ohio State University, Columbus, OH 43210
Received 1996 August 12; accepted 1996 November 4

ABSTRACT

The total and state-specific electron-ion recombination rate coefficients are obtained for Fe I. The calculations are carried out using a new ab initio method that incorporates both the radiative and the dielectronic recombination processes in an unified and self-consistent manner. The computations employ the close coupling approximation and the *R*-matrix method from atomic collision theory. A 52 state close coupling eigenfunction expansion dominated by the states of the ground $3d^64s$ and excited $3d^7$, $3d^64p$, $3d^54s^2$, and $3d^54s4p$ configurations of Fe II are used in the present calculations. The important electron correlation and radiation damping effects are included via explicit coupling of autoionization and radiative channels. This is the first detailed atomic calculation for the recombination rates for Fe I. The present rates are considerably higher than the radiative recombination rates being used currently in the low-temperature region, $T \leq 10^4$ K, whereas they are about 4 times lower than those given by the Burgess general formula for dielectronic recombination at higher temperatures. The implications of the new recombination rate coefficients and photoionization cross sections for Fe I on the ionization structure of iron in the cold neutral interstellar medium are studied. It is found that the ratio of Fe II to Fe I obtained with the new atomic data increases by a factor of about 3–30 over previous calculations.

Subject headings: atomic data — atomic processes — ISM: abundances

1. INTRODUCTION

Fe I is an important constituent of cold and/or dense astronomical sources such as H II/H I regions, the neutral interstellar medium (ISM), and stellar atmospheres. In these sources the ionization of Fe plays an important role in the heating of the gas. Consequently, the emission spectra of Fe I and Fe II may be of importance in the cooling of the ambient medium. Knowledge of accurate recombination rate coefficients, as well as accurate photoionization cross sections *consistent* with the recombination rates, is then necessary for the computation of the ionization and thermal balance of the gas (Wolfire et al. 1995). Fe I is also present in the spectra of stellar atmospheres, e.g., in the Sun (Bell, Paltoglou, & Tripicco 1994). For many stars, non-LTE (NLTE) effects are known to be very important (see Dreizler & Werner 1993; Hubeny & Lanz 1996); however, heretofore no accurate NLTE treatment of Fe I has been possible because of the absence of state specific photoionization cross sections and recombination rate coefficients.

Prior to the development of a unified approach to electron-ion recombination (Nahar & Pradhan 1992, 1994, 1995, hereafter NP1, NP2, NP3, respectively), calculations for electron-ion recombination usually treated the radiative and the dielectronic recombination (RR and DR) processes separately using different approximations, valid in different temperature regions and are thus susceptible to inconsistencies and inaccuracies when simply added together to obtain the total recombination rate. Furthermore, they are not, in general, consistent with the photoionization cross sections, which are usually calculated in some other approximation. Ionization balance calculations in photoionization models of radiatively ionized astrophysical plasma sources are therefore subject to large uncertainties, particularly for complex atomic systems such as the low-ionization stages of iron. The RR and the DR rates for iron have been given by Woods, Shull, & Sarazin (1981). The RR rates were obtained from the photoionization cross sections calculated in central field approximation (Reilman & Manson 1979) and in hydrogenic approximations. For the DR rates, Woods et al. (1981) employed the Burgess general formula (BGF; see Burgess 1965) using the then available oscillator strengths. In a later work, Hahn (1989) calculated the DR rates using an improved empirical formula based on the BGF; however, there was no accurate atomic data available for Fe I at that time for the empirical formula.

The present work reports detailed calculations for electron-ion recombination rates for e + Fe II → Fe I using the new unified treatment (NP1, NP2, NP3), which combines the two recombination processes, RR and DR, and yields a single set of unified recombination rate coefficients over a wide range of temperatures for all practical purposes. The calculations are carried out in the close coupling (CC) approximation using the *R*-matrix method. A previous application of this method to complex systems with strong electron correlations and a large number of recombination channels was reported by Nahar (1996) for e + Fe IV → Fe III. The photoionization cross sections for Fe I, also calculated in the CC approximation with the same 52 state eigenfunction expansion as in the present recombination work, are being reported separately by Bautista (1996) as part of the Iron Project (Hummer et al. 1993).

2. SUMMARY OF THE THEORETICAL WORK AND COMPUTATIONS

The theoretical details of the unified treatment for total electron-ion recombination rate coefficients are given in NP2 and NP3. In the unified treatment, the infinite number of final recombined states are divided into two groups: (A) low-n states that correspond to all bound states with principal quantum number $n \leq n_{\max}$ and (B) high-n states with $n_{\max} \leq n \leq \infty$. Recombination via group A states is considered explicitly through detailed calculations of photoionization cross sections with autoionization structures, whereas recombination via group B states is considered

using an extension of the precise theory of DR by Bell & Seaton (1985; see also NP2). Some computational details and important features of the calculations are presented below.

2.1. *Low-n States: Partial Photoionization Cross Sections*

For all bound states of group A, the partial photoionization cross sections, $\sigma_{\rm PI}(g)$, for photoionization into the ground state (g) of the residual core ion are calculated. There are 430 bound states of Fe I obtained in the present calculation that couple to the ^6D ground state of Fe II with $n_{\rm max} = 10$ and $\ell_{\rm max} = 7$. Calculations of $\sigma_{\rm PI}(g)$ are carried out in the (CC) approximation employing the R-matrix package of codes developed for the Opacity Project (Berrington et al. 1987) and extended for the Iron Project (Hummer et al. 1993). All autoionizing resonances in the cross sections with effective quantum number ν up to 10.0 are resolved in detail. We employ a 52 state eigenfunction expansion of Fe II with states dominated by the ground $3d^64s$ and excited $3d^7$, $3d^64p$, $3d^54s^2$, and $3d^54s4p$ configurations, ensuring inclusion of the important electron correlation effects as explained in Bautista & Pradhan (1995). Further details of the wave function expansion and the computations of the photoionization cross sections are given in Bautista (1996).

It should be noted that out of 430 calculated bound states, only 65 LS states have been observed. Identification of the calculated states were carried out through determination of the quantum defects and channel wave function contributions using the code ELEVID (Nahar 1995). It requires large eigenfunction expansions and inclusion of extensive correlations to obtain the large number of closely spaced energy levels of complex atoms. However, even with the extensive eigenfunction expansion and consequently huge investment of CPU time and memory, some of the high-lying states may not be well represented, because of strong admixture of states of the same angular and spin symmetries. Identification of such states is therefore rendered difficult, since the quantum defect series and the channel wave functions are strongly perturbed. The computational spectroscopy problems encountered in this work, and similar calculations for other heavy elements, are not unlike those in the identification of laboratory spectra.

The recombination cross sections are obtained from the $\sigma_{\rm PI}(g)$ values through the Milne relation (NP3). Since the $\sigma_{\rm PI}(g)$ values include the autoionizing resonance profiles with the coupled background continua, the recombination rate coefficients obtained from these cross sections subsume both the RR and the DR processes. The contributions from the 430 low-n bound states to the total recombination rate coefficient, α_R, correspond to the sum of the state-specific rates of all these bound states. Not all the states have significant contributions to the total rates. A limited number of states provide dominant contribution individually to the total rates. The number of dominant states and the order of their contributions vary with temperature because of energy dependence of resonance structures in the photoionization cross sections.

The recombination rate coefficients are obtained using the code RECOMB (Nahar 1996). A few important points can be noted concerning the contributions of the photoionization cross sections to the total recombination rate coefficients, α_R. For simple ions, it is often the ground state of the recombined ion that dominates the recombination rates. For Fe I, however, recombination to several excited states dominates the total recombination rate. The reason is that the low-lying excited states of Fe I have larger effective cross sections than the ground state, as shown in Figures 1 and 2. Figure 1 presents the partial photoionization cross sections of the first two lowest states of Fe I: (*a*) the ground state $3d^64s^2(^5D)$ and (*b*) the first excited $3d^74F4s(^5F)$ state. The ground state cross section shows extensive resonances in the low-energy region, but the effective cross section falls to about 10^{-1} mbar in the higher energy region, in which the ^5F cross section is much higher.

Figure 2 presents partial photoionization cross sections of three excited states of Fe I: (*a*) $3d^64s\,^6D4p(^5D^o)$, (*b*) $3d^64s\,^6D4p(^7F^o)$, and (*c*) $3d^64s\,^6D6p(^5F^o)$. The figure shows that both the $^5D^o$ and the $^7F^o$ have greater effective cross sections than the ground state ^5D of Figure 1*a*. These two are among the excited states that dominate the recombination at temperatures up to about 10,000 K.

Figure 2*c* illustrates an important feature known as the photoexcitation of core (PEC) resonances. These large and very wide resonances occur at energies corresponding to strong dipole allowed transitions in the core ion, primarily from the ground state (so-called resonance transitions). The PEC phenomenon is the inverse of the DR process, with the outer electron being essentially a "spectator" during excitation of the core by the incident photon. In Figure 2*c* the effective cross section of $^5F^o$ is seen to fall from its threshold value until the photon energy reaches the excitation energies from the ^6D ground state of the Fe II core ion to the excited odd-parity states $^6D^o$ at 0.349 ryd, $^6F^o$ at 0.380 ryd,

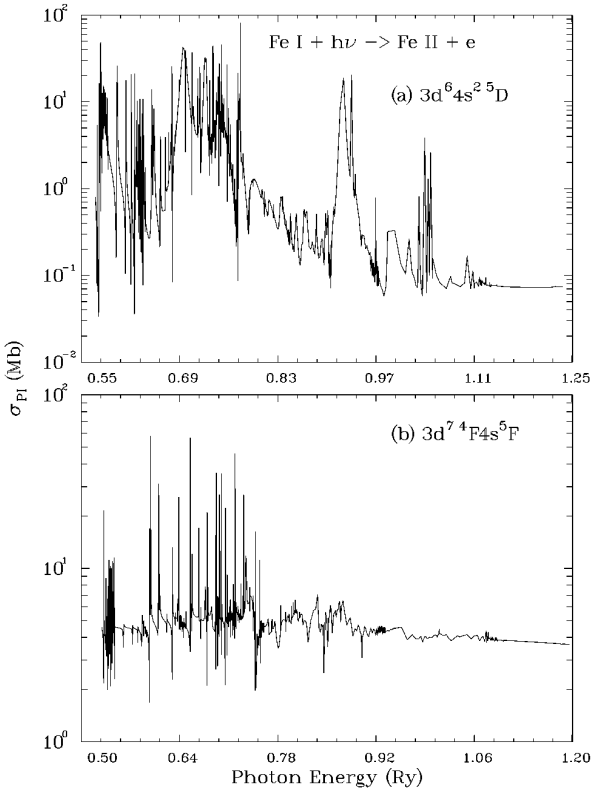

FIG. 1.—Partial photoionization cross sections of the lowest two states: (*a*) the ground state $3d^54s^2(^5D)$ and (*b*) the $3d^6s(^5F)$ states of Fe I.

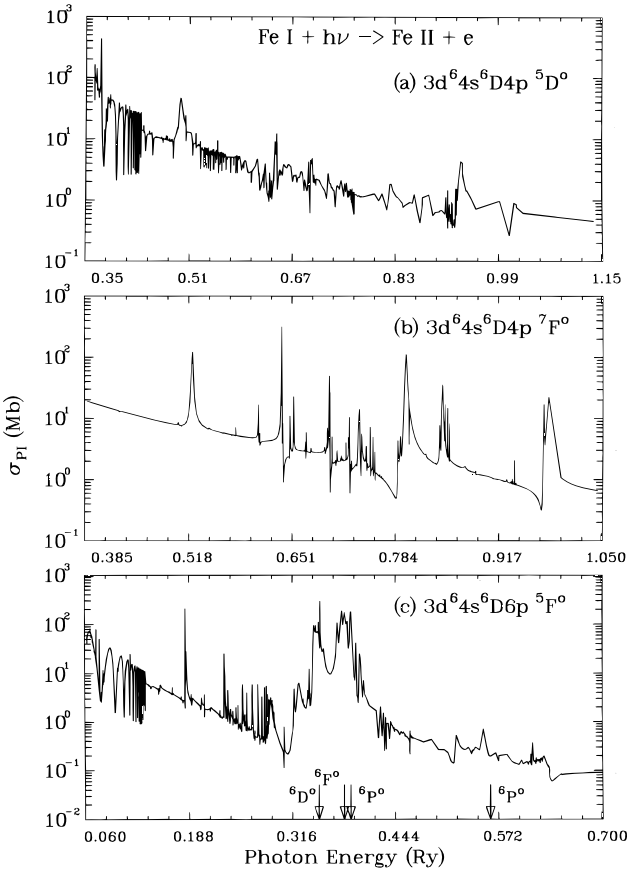

FIG. 2.—Partial photoionization cross sections of three excited states of Fe I: (*a*) $3d^6 4s\,^6D4p(^5D^o)$, (*b*) $3d^6 4s\,^6D4p(^7F^o)$, and (*c*) $3d^6 4s\,^6D6p(^5F^o)$ of Fe I. The arrows in (*c*) indicate positions of dipole allowed transitions in the core where the PEC resonances are formed.

$^6P^o$ at 0.389 ryd, and $^6P^o$ at 0.562 ryd (shown by arrows in the figure), where the large PEC resonances are formed. The PEC resonances manifest themselves strongly in the photoionization cross section of excited bound states, attenuating the background cross section by orders of magnitude. Consequently, the photoionization cross section of excited states of atoms deviates considerably from hydrogenic values. Therefore, the use of the widely employed hydrogenic or central field approximations to compute excited state cross sections is incorrect since the strong coupling effects of the core electrons, as seen via the PEC resonances, are neglected.

2.2. *High-n States: Collision Strengths for Dielectronic Recombination*

For the group B states ($n_{\max} < n \leq \infty$), electron-ion recombination is dominated by DR since the background contribution is negligibly small because of high principal quantum numbers; the density of states per unit energy interval increases as ν^3, and the autoionization decay rate decreases as ν^{-3}. In the energy range corresponding to the high-*n* levels (referred to as the QDT region since the theoretical methods are based on multichannel quantum defect theory), the collision strengths for DR are obtained in the CC approximation employing the theory developed by Bell and Seaton (Bell & Seaton 1985; NP2; Nahar 1996). The calculations are carried out using the *identical* 52 state eigenfunction expansion used for the photoionization cross sections. The *R*-matrix code STGF for the calculation of asymptotic wave functions has been extended for the DR calculations, and the new code is known as STGFDR (NP2). Transition probabilities for the dipole allowed transitions in Fe II are obtained from the *f* values of NP2; these are given in Table 1. The convergence of the *R*-matrix basis set within the *R*-matrix boundary was checked by comparing the threshold collision strengths for electron impact excitation with and without the inclusion of long-range multipole potentials in the asymptotic part of the wave functions (NP2). The calculations yield good agreement between the electron impact collision strengths at these thresholds, ensuring the validity of the DR calculations in the aforementioned QDT region (this point is discussed in NP2 and NP3).

The detailed and the resonance-averaged DR collision strengths Ω(DR) for e + Fe II → Fe I are shown in Figure 3. The Rydberg series of resonances converging onto the three dipole allowed excited thresholds $^6D^o$, $^6F^o$, and $^6P^o$ are represented by the dotted line, while the resonance averaged collision strengths are denoted by the solid line [Ω(DR) below the next $^6P^o$ state is not shown as this state lies rather high in energy]. It can be seen that as the effective quantum number increases, the DR resonances get narrower and denser, achieving peak values at the said thresholds. This pattern is seen more distinctly in the solid line that shows the resonance-averaged collision strengths, which rise sharply as they approach the excited thresholds. The peak value of the $\langle\Omega(\mathrm{DR})\rangle$ at the thresholds for the four dipole allowed transitions are given in Table 1. The filled circles in Figure 3 correspond to the excitation collision strengths, Ω_{EIE}, at the first three excited thresholds. Independent CC calculations are carried out employing the same 52 state eigenfunction expansion for the excitation collision strengths at the thresholds for the dipole transitions within the core ion. It is expected that Ω(DR) and Ω_{EIE} should agree if the flux is to be conserved; the photon flux due to DR just below the threshold should equal the scattered electron flux at the threshold. However, the situation may be complicated if there exist strongly overlapping resonance structures converging onto more than one threshold of the target ion. In the present calculations, good agreement is obtained for two of the thresholds of Fe II (Table 1), but the first two transitions show a significant discrepancy. Nonetheless, the DR contribution to the total recombination rate coefficient is not affected much, i.e., the effect is less than the estimated uncertainties, 10%–30%, in the calculations.

Contributions from the high-*n* states to the total α_R are obtained from the averaged DR collision strengths, $\langle\Omega(\mathrm{DR})\rangle$. In computing the $\langle\Omega(\mathrm{DR})\rangle$ values, the detailed Ω(DR) must be calculated with a very fine mesh such that all resonance structures are adequately resolved. The back-

TABLE 1

TRANSITION PROBABILITIES, A_{ji}, AND COLLISION STRENGTHS OF BOTH Ω_{EIE} AND Ω(DR) AT EXCITED THRESHOLDS OF Fe II

Transition	A_{ji} (a.u.)	Ω_{EIE}	Ω(DR)
a	5.96-9	48.35	40.68
$a\ \mathrm{D}^{e6} \rightarrow z\ \mathrm{F}^{o6}$	6.79-9	45.68	53.46
$a\ \mathrm{D}^{e6} \rightarrow z\ \mathrm{P}^{o6}$	5.21-9	12.65	12.30
$a\ \mathrm{D}^{e6} \rightarrow y\ \mathrm{P}^{o6}$	7.12-9	0.841	0.840

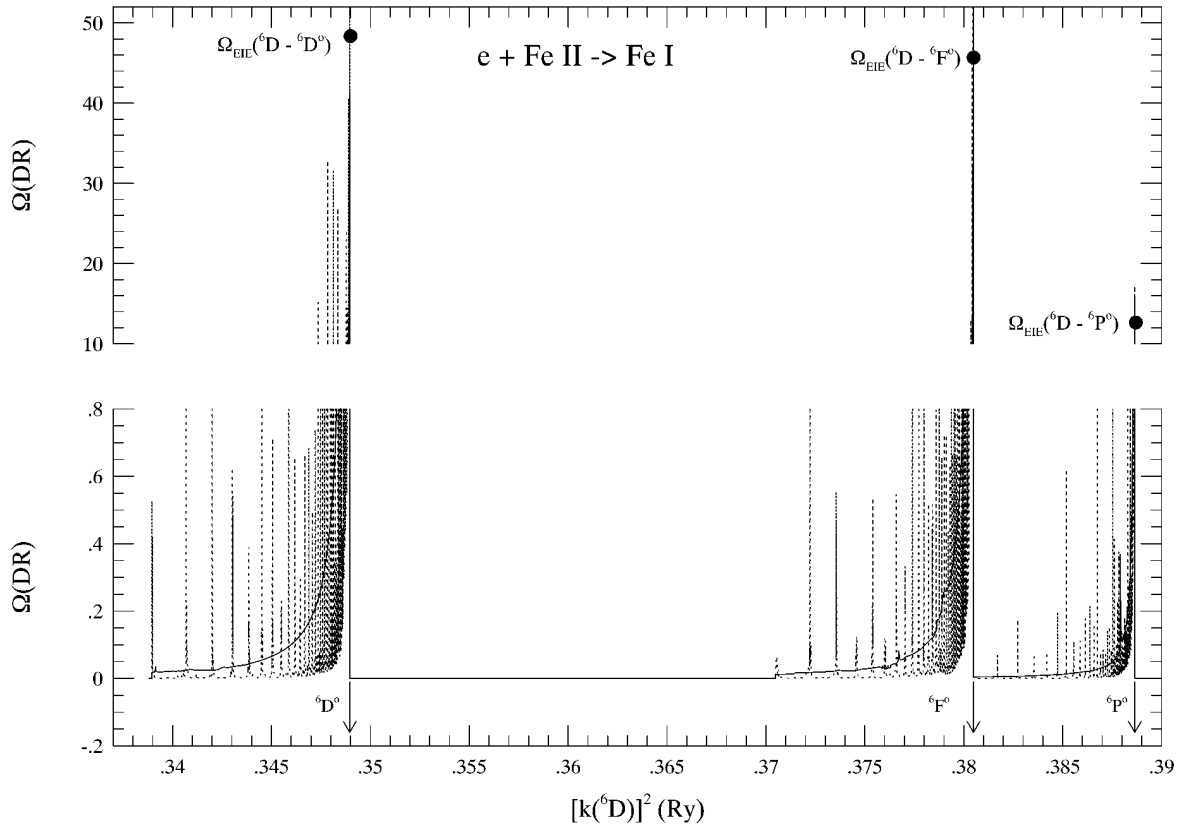

FIG. 3.—Collision strengths for DR, detailed with resonances (*dotted lines*) and averaged over resonances (*solid lines*). The filled circles correspond to excitation collision strengths at the thresholds specified.

ground RR through the high-n states is also included in the calculation of the total recombination rate coefficients in a hydrogenic "top-up" scheme, as explained in Nahar (1996). These contributions are, of course, significant in the very low temperature regime (Fig. 4), in which resonant recombinations are energetically inaccessible.

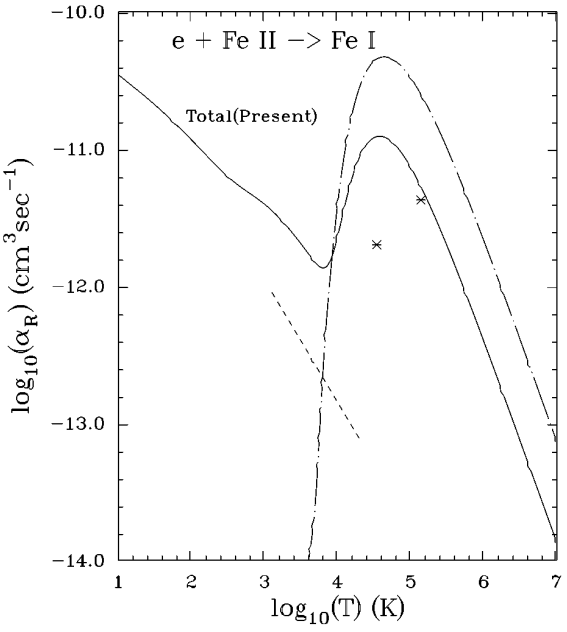

FIG. 4.—Total recombination rate coefficients, $\alpha_R(T)$ (*solid line*), for e + Fe II → Fe I. The dashed line corresponds to RR, and the dot-dashed line to DR rates of Woods et al. (1981); the asterisks correspond to the DR rates by Hahn (1989).

3. RESULTS AND DISCUSSION

The present work yields the total e + Fe II → Fe I recombination rate coefficients, as well as state-specific recombination rates for a number of low-n bound states of Fe I. Table 2 presents the state-specific recombination rate coefficients at temperatures T = 10, 100, 1000, and 10,000 K. The table lists the top 20 bound states of Fe I in order of their contributions to the total recombination rate coefficient, α_R, given at the bottom of the table. The order of the dominant states, and their fractional (percentage) contributions to the total α_R, varies with temperature, primarily because of detailed autoionization structures of resonances in the corresponding photoionization cross sections. It might be noted that the ground state ^5D of Fe I is not the dominant recombining state at the temperatures given (as discussed in § 2.1). Some uncertainty in the state-specific recombination rate coefficients might exist in the limits of very low and very high temperatures. At very low temperatures the coefficients are very sensitive to the exact positions and widths of the resonances. For very high temperatures the uncertainties may arise from the fact that the DR contributions of highly excited core levels are not considered (the latter uncertainty would be negligible at temperatures at which Fe I is likely to be abundant).

The values of the total $\alpha_R(T)$ are presented in Table 3 for the temperature range of $1.0 \leq \log_{10}(T) \leq 7.0$ with a mesh of $\Delta \log_{10}(T) = 0.1$ for easy interpolation. The total $\alpha_R(T)$ is also plotted in Figure 4 (*solid line*). The α_R curve is seen to decay smoothly with temperature up to $T \sim 10^4$ K. After

TABLE 2

RECOMBINATION RATE COEFFICIENTS[a]

10 K		100 K		1000 K		10000 K	
State	α_R	State	α_R	State	α_R	State	α_R
$3d^64s\,^6D^e4p(^7F^o)$	1.93-12	$3d^64s\,^6D^e4p(^5D^o)$	1.46-12	$3d^64s\,^6D^e4p(^5F^o)$	6.63-13	$3d^64s\,^6D^e4p(^5F^o)$	9.75-14
$3d^64s\,^6D^e4p(^7D^o)$	1.88-12	$3d^64s\,^6D^e4p(^5F^o)$	1.05-12	$3d^64s\,^6D^e4p(^5P^o)$	3.77-13	$3d^64s\,^4D^e4p(^5F^o)$	5.78-14
$3d^64s\,^6D^e4p(^5D^o)$	1.39-12	$3d^64s\,^6D^e4p(^7F^o)$	6.13-13	$3d^64s\,^6D^e4p(^5D^o)$	3.66-13	$3d^64s\,^6D^e4p(^5P^o)$	5.64-14
$3d^64s\,^4D^e4p(^5F^o)$	1.14-12	$3d^64s\,^6D^e4p(^7D^o)$	5.81-13	$3d^64s\,^6D^e4p(^7F^o)$	1.89-13	$3d^64s\,^6D^e4p(^7F^o)$	5.55-14
$3d^64s\,^6D^e4p(^7P^o)$	9.72-13	$3d^64s\,^6D^e4p(^5P^o)$	4.63-13	$3d^64s\,^6D^e4p(^7D^o)$	1.69-13	$3d^64s\,^6D^e4p(^5D^o)$	5.24-14
$3d^64s\,^6D^e4p(^5F^o)$	7.24-13	$3d^64s\,^4D^e4p(^5F^o)$	3.08-13	$3d^7\,^4F^e4p(^5F^o)$	1.22-13	$3d^64s\,^6D^e4p(^7D^o)$	4.39-14
$3d^7\,^4F^e4s(^5F^e)$	6.15-13	$3d^64s\,^6D^e4p(^7P^o)$	3.05-13	$3d^64s\,^4D^e4p(^5F^o)$	9.44-14	$3d^64s\,^4D^e4p(^5D^o)$	3.14-14
$3d^7\,^4F^e4p(^5G^o)$	4.26-13	$3d^7\,^4F^e4s(^5F^e)$	1.89-13	$3d^64s\,^6D^e4p(^7P^o)$	9.29-14	$3d^7\,^4F^e4p(^5F^o)$	2.91-14
$3d^64s\,^6D^e4p(^5P^o)$	3.41-13	$3d^7\,^4F^e4p(^5G^o)$	1.36-13	$3d^7\,^4F^e4s(^5F^e)$	6.58-14	$3d^7\,^4F^e4s(^5F^e)$	2.76-14
$3d^64s\,^6D^e5p(^7F^o)$	2.65-13	$3d^64s\,^4D^e4p(^5D^o)$	1.18-13	$3d^7\,^4F^e4p(^5G^o)$	6.33-14	$3d^64s\,^4D^e4p(^5P^o)$	2.75-14
$3d^64s\,^6D^e4d(^7G^e)$	2.56-13	$3d^7\,^4F^e4p(^5F^o)$	1.05-13	$3d^64s\,^4D^e4p(^5D^o)$	5.69-14	$3d^64s\,^6D^e4p(^7P^o)$	2.64-14
$3d^64s\,^6D^e4d(^5G^e)$	2.38-13	$3d^64s\,^4D^e4p(^5P^o)$	9.50-14	$3d^7\,^4F^e4p(^5D^o)$	4.77-14	$3d^7\,^4F^e4p(^5D^o)$	2.47-14
$3d^64s\,^6D^e4d(^7F^e)$	2.23-13	$3d^64s\,^6D^e5p(^7F^o)$	8.38-14	$3d^64s2(^5D^e)$	4.67-14	$3d^64s2(^5D^e)$	1.88-14
$3d^64s\,^6D^e5p(^7D^o)$	2.05-13	$3d^64s\,^6D^e4d(^7G^e)$	8.04-14	$3d^64s\,^4D^e4p(^5P^o)$	3.77-14	$3d^64s\,^6D^e5p(^7F^o)$	1.63-14
$3d^64s\,^6D^e5p(^5F^o)$	1.82-13	$3d^64s\,^6D^e4d(^5G^e)$	7.48-14	$3d^7\,^4P^e4s(^5P^e)$	3.76-14	$3d^7\,^4P^e4s(^5P^e)$	1.50-14
$3d^64s\,^6D^e4d(^7D^e)$	1.52-13	$3d^64s\,^6D^e4d(^7F^e)$	7.03-14	$3d^64s\,^4P^e4p(^5D^o)$	3.16-14	$3d^64s\,^6D^e4d(^7G^e)$	1.40-14
$3d^64s\,^6D^e5d(^7G^e)$	1.48-13	$3d^64s\,^4D^e5p(^5F^o)$	6.91-14	$3d^64s\,^4P^e4p(^5P^o)$	2.66-14	$3d^64s\,^6D^e5s(^7D^e)$	1.37-14
$3d^7\,^4P^e4s(^5P^e)$	1.47-13	$3d^64s\,^6D^e5p(^7D^o)$	6.51-14	$3d^64s\,^6D^e5p(^7F^o)$	2.60-14	$3d^7\,^4F^e4p(^5G^o)$	1.21-14
$3d^64s\,^6D^e5p(^5D^o)$	1.41-13	$3d^64s\,^6D^e5p(^5F^o)$	6.14-14	$3d^64s\,^4D^e5p(^5F^o)$	2.44-14	$3d^64s\,^6D^e4d(^7F^e)$	1.19-14
$3d^7\,^4F^e4p(^5F^o)$	1.28-13	$3d^64s\,^6D^e4d(^7D^e)$	4.73-14	$3d^64s\,^6D^e4d(^7G^e)$	2.36-14	$3d^64s\,^4P^e4p(^5D^o)$	1.02-14
Sum	1.15-11		5.98-12		2.56-12		6.42-13
Total	3.48-11		1.16-11		3.95-12		2.30-12
Contribution (%).....	33%		52%		65%		28%

[a] Recombination rate coefficients (in units of $cm^3\ s^{-1}$) of the top 20 individual states of Fe I in order of their contributions to the total α_R at temperatures $T = 10$, 100, 1000, and 10,000 K.

this point α_R rises again because of the dominance of DR at higher temperatures. An interesting feature of the α_R (Fe I) is the bump that appears from about 400 K to 6000 K. This low-T bump arises because of enhancement in the recombination rates by the low-energy autoionizing resonances in the photoionization cross sections. Similar kind of bumps have been observed in other ions, such as O III (Nussbaumer & Storey 1983; NP1). The recombination rates of Fe III also show such a low-T bump (Nahar 1996).

Figure 4 compares the present $\alpha_R(T)$ with previous results by Woods et al. (1981) (*dashed line* for RR; *dot-dashed line* for DR) and with the DR rates of Hahn (1989; *asterisks*). It is noted that the present rates are considerably higher than previous RR rates in the low-T region, whereas for higher temperatures the present results are about 4 times lower than those of Woods et al. (1981). The reasons for these differences are clear. For low temperatures, Woods et al. (1981) calculated the recombination rates for RR using the photoionization cross section for the Fe I ground state by Reilman & Manson (1979), and cross sections for the first excited subshells obtained from extrapolation of the same Reilman and Manson data. However, the new, accurate photoionization cross sections for the ground and excited states of Fe I (Bautista 1996) differ from those of Reilman & Manson (1979) by up to *3 orders of magnitude* or more (Bautista & Pradhan 1995; Bautista 1996). Also, in the region near the ionization threshold, the new photoionization cross sections contain complex structures of autoionization resonances that lead to considerable enhancement of electron-ion recombination in the present unified method; these resonances are absent from the cross sections by Reilman & Manson (1979), which represent only the background. For higher temperatures, the DR rates of Woods et al. (1986) were calculated using the BGF (Burgess 1965), with oscillator strengths given by de Boer et al. (1974) for Fe II. In general, the BGF is not likely to yield accurate DR rates for complex systems such as Fe I, which, as we have shown, involve complicated coupling effects between a large number of autoionization and radiative channels and associated resonance profiles. As the autoionization into the lower excited states reduces the DR, as first noted by Jacobs et al. (1977), BGF usually overestimates the DR rates. Figure 4 also compares the present rates with the DR rates from the empirical formula of Hahn (1989) at two temperatures. These rates do not show any specific pattern. The high-T value of Hahn agrees reasonably well with the present values, but the low-T value is considerably lower, possibly because of low-energy resonant recombinations included in the present work. (Fe I is one of the gap ions for which no reliable atomic data were available for the empirical formula.)

The present values of $\alpha_R(T)$ should be accurate to within 10%–30% for most of the temperature range of practical importance, up to an excitation temperature of 10^5 K corresponding to the highest target state $3d^54s^2(^4F)$ at 0.67 ryd in the CC expansion. The estimate of accuracy is based on the general accuracy of the CC method for photoionization cross sections and electron scattering and DR collision strengths. At high temperatures ($T > 10^5$ K), the rates may be more uncertain because of possible recombinations via bound states formed with the omitted target states. However, for neutral and near-neutral atomic systems, such doubly excited states are usually autoionizing. Furthermore, the contribution of these highly excited states to high-temperature rates is small because the DR collision strengths decrease with increasing energy and "n," autoionization into the lower coupled excited states, weaker PEC resonances, and exponential Maxwellian damping. We further note that with a large target expansion, the background cross sections of comparatively highly excited states

TABLE 3

TOTAL RECOMBINATION RATE COEFFICIENTS[a]

$\log_{10} T$	α_R
1.0	3.48-11
1.1	3.14-11
1.2	2.84-11
1.3	2.58-11
1.4	2.33-11
1.5	2.09-11
1.6	1.87-11
1.7	1.67-11
1.8	1.48-11
1.9	1.31-11
2.0	1.16-11
2.1	1.02-11
2.2	9.02-12
2.3	7.97-12
2.4	7.04-12
2.5	6.27-12
2.6	5.65-12
2.7	5.15-12
2.8	4.73-12
2.9	4.34-12
3.0	3.95-12
3.1	3.55-12
3.2	3.14-12
3.3	2.75-12
3.4	2.37-12
3.5	2.02-12
3.6	1.72-12
3.7	1.47-12
3.8	1.35-12
3.9	1.52-12
4.0	2.30-12
4.1	3.89-12
4.2	6.19-12
4.3	8.72-12
4.4	1.09-11
4.5	1.21-11
4.6	1.24-11
4.7	1.17-11
4.8	1.05-11
4.9	8.95-12
5.0	7.35-12
5.1	5.86-12
5.2	4.56-12
5.3	3.48-12
5.4	2.62-12
5.5	1.95-12
5.6	1.43-12
5.7	1.05-12
5.8	7.61-13
5.9	5.51-13
6.0	3.95-13
6.1	2.83-13
6.2	2.03-13
6.3	1.45-13
6.4	1.04-13
6.5	7.38-14
6.6	5.26-14
6.7	3.74-14
6.8	2.66-14
6.9	1.90-14
7.0	1.35-14

[a] Total recombination rate coefficients $\alpha_R(T)$ (in units of $cm^3\ s^{-1}$) for $e + \text{Fe II} \rightarrow \text{Fe I}$ for a temperature T(K) range of $1.0 \leq \log_{10}(T) \leq 9.0$.

show relatively little resonance structures long before the highest target threshold. Hence, the extrapolation of the background cross sections to high energies (Nahar & Pradhan 1994) and the tabulated rates for $T > 10^5$ K should be reasonably accurate, although with somewhat higher uncertainty.

4. IONIZATION BALANCE OF Fe I/Fe II IN H II/H I REGIONS

In this section we illustrate the possible consequences of the new photoionization cross sections and recombination rates for Fe I/Fe II on the ionization balance of iron in the cold neutral interstellar medium. The new atomic data yields a Fe II/Fe I ratio that is 3–30 times greater than that obtained in previous calculations. For this study, we calculate photoionization rates using the "standard" UV background radiation field in the ISM given by Draine (1978) in the photon energy range 5–13.6 eV.

The photoionization rate of Fe I (Γ) is given by

$$\Gamma(s^{-1}) = 4\pi \int_{E_0}^{13.6\ \text{eV}} F(E)\sigma_E\, dE\ , \qquad (1)$$

where σ_E is the total ground state photoionization cross section in cm^2, E_0 is the ionization potential of Fe I (= 7.9 eV). The empirically derived function $F(E)$ has the following form (Draine 1978):

$$F(E) = 1.658 \times 10^6 (E/\text{eV}) - 2.152 \times 10^5 (E/\text{eV})^2 + 6.919 \times 10^3 (E/\text{eV})^3\ , \qquad (2)$$

in units of photons $cm^{-2}\ sr^{-1}\ s^{-1}\ eV^{-1}$.

Using the photoionization cross section for the ground state of Fe I from Bautista & Pradhan (1995) and Bautista (1996), one obtains $\Gamma = 1.21 \times 10^{-9}\ s^{-1}$. On the other hand, if the photoionization cross section from Reilman & Manson (1979) is used instead, then the ionization rate would be underestimated by nearly a factor of 30, with $\Gamma = 4.39 \times 10^{-11}\ s^{-1}$. A much better choice of the cross section than that of Reilman & Manson (1979) is the cross section calculated by Kelly (1972), as used by de Boer, Koppenaal, & Pottasch (1973). However, the absence of much of the resonance structures in Kelly's cross sections also leads to an to an underestimation of the ionization rate by more than a factor of 3, with $\Gamma = 3.8 \times 10^{-10}\ s^{-1}$.

Morton (1975) has reported the simultaneous detection of Fe I and Fe II lines in the direction of ψ Oph. Three different determinations of the temperature in the H I cloud were presented by Morton: a kinematic temperature of $T = 56°$ K originally derived by Spitzer et al. (1974), $T = 94°$ K obtained by fitting the observed level populations of H_2, and $T = 19°$ K derived from the fine-structure lines of C I. The present recombination rate coefficients α_R of Fe I at these temperatures are 1.58×10^{-11}, 1.18×10^{-11}, and $2.63 \times 10^{-11}\ s^{-1}\ cm^{-3}$, respectively, whereas the recombination rate coefficients by Woods et al. (1981) are 1.44×10^{-11}, 0.91×10^{-11}, and $3.78 \times 10^{-11}\ s^{-1}\ cm^{-3}$. Given the ionization and recombination rates, the ratio of Fe II to Fe I in the H I cloud can be readily computed for any electron density (N_e) according to the relation

$$\frac{N(\text{Fe II})}{N(\text{Fe I})} = \frac{1}{N_e}\frac{\Gamma}{\alpha_R}\ . \qquad (3)$$

Conversely, the ratio of Fe II to Fe I can be derived directly from observations, as in Morton (1975), and the electron

density of the region can be calculated. Thus, assuming a mean value for $N(\text{Fe II})/N(\text{Fe I}) \sim 1100$, as derived by Morton, one gets $N_e = 0.069, 0.093, 0.041\ \text{cm}^{-3}$ for $T = 56$, 94, 19 K, respectively. If, however, ionization rates obtained from the cross sections by Kelly (1972) and recombination coefficients by Woods et al. (1981) had been used, then one would get significantly lower electron densities: $N_e = 0.024$, $0.038, 0.009\ \text{cm}^{-3}$). The use of Reilman & Manson (1979) cross section to compute the ionization rate would yield far lower, and possibly unrealistic, electron densities. Clearly, the new iron data should lead to a significant revision of heating and cooling rates and density determinations in the cold ISM (Wolfire et al. 1995).

In addition to the importance of using a consistent set of photoionization and recombination data, the above analysis also emphasizes the importance of autoionization resonances to the total photoionization rate. As such, simple fits to cross sections neglecting the detailed autoionization profiles, particularly in the near-threshold regions, may lead to substantial error in the computation of photoionization equilibria.

5. CONCLUSION

Total recombination rate coefficients are obtained for neutral iron and are tabulated over a wide range of temperatures. The present results are considerably higher for $T \leq 10^2$ K than those by Woods et al. (1981), and for higher temperatures, they are about 4 times lower. We expect the present recombination coefficients to be accurate to about 10%–30% in the temperature region of Fe I abundance.

The implications of the new recombination rate coefficients and photoionization cross sections on the ionization structure of iron in the cold neutral ISM are studied, and it is found that the ratio of Fe II to Fe I obtained with the new atomic data increases by a factor of about 3–30 over previous calculations.

It might also be emphasized that, for the first time, a self-consistent set of photoionization and recombination data is presented for calculations involving radiative equilibrium in plasmas. Similar calculations for other ions of iron, as well as for other astrophysically abundant elements such as carbon, nitrogen and oxygen, are in progress. Both the photoionization and the recombination data are available from the first author at nahar@payne.mps.ohio-state.edu.

The work has been supported by NSF grant PHY-9421898 and NASA grants NAGW-3315 and NAS-32643. The computational work was carried out on the Cray YMP at the Ohio Supercomputer Center.

REFERENCES

Bautista, M. A. 1996, A&AS, in press
Bautista, M. A., & Pradhan, A. K. 1995, J. Phys. B, 28, L173
Bell, R. A., Paltoglou, G., & Tripicco, M. J. 1994, MNRAS, 268, 771
Bell, R. H., & Seaton, M. J. 1985, J. Phys. B, 18, 1589
Berrington, K. A., Burke, P. G., Butler, K., Seaton, M. J., Storey, P. J., Taylor, K. T., & Yan, Y. 1987, J. Phys. B, 20, 6379
Burgess, A. 1965, ApJ, 141, 1588
de Boer, K. S., Koppenaal, K., & Pottasch, S. R. 1973, A&A, 28, 145
de Boer, K. S., Morton, D. C., Pottasch, S. R., & York, D. G. 1974, A&A, 31, 405
Draine, B. T. 1978, ApJS, 36, 595
Dreizler, S., & Werner, K. 1993, A&A, 278, 199
Hahn, Y. 1989, J. Quant. Spectrosc. Radiat. Transfer, 41, 315
Hubeny, I., & Lanz, T. 1996, in Astrophysics in the Extreme Ultraviolet, ed. S. Bowyer & R. F. Malina (Dordrecht: Kluwer), 381
Hummer, D. G., Berrington, K. A., Eissner, W., Pradhan, A. K., Saraph, H. E., & Tully, J. A. 1993, A&A, 279, 298
Jacobs, V. L., Davis, J., Kepple, P. C., & Blaha, M. 1977, ApJ, 211, 605
Kelly, H. P. 1972, Phys. Rev. A, 6, 1048
Morton, D. C. 1975, ApJ, 197, 85
Nahar, S. N. 1995, A&A, 293, 967
———. 1996, Phys. Rev. A, 53, 2417
Nahar, S. N., & Pradhan, A. K. 1992, Phys. Rev. Lett., 68, 1488 (NP1)
———. 1994, Phys. Rev. A, 49, 1816 (NP2)
———. 1995, ApJ, 447, 966 (NP3)
Nussbaumer, H., & Storey, P. J. 1983, A&A, 126, 75
Reilman, R. F., & Manson, S. T. 1979, ApJS, 40, 815
Spitzer, L., Cochran, W. D., & Hirshfeld, A. 1974, ApJS, 28, 373
Wolfire, M. G., Hollembach, D., McKee, C. F., Tielens, A. G. G., & Bakes, E. L. O. 1995, ApJ, 443, 152
Woods, D. T., Shull, J. M., & Sarazin, C. L. 1981, ApJ, 249, 399